Conf-950740--26
SAND95-0582C

DYNAMIC PULSE BUCKLING OF CYLINDRICAL SHELLS UNDER AXIAL IMPACT: A BENCHMARK STUDY OF 2D AND 3D FINITE ELEMENT CALCULATIONS†

Edward L. Hoffman
Engineering and Manufacturing Mechanics Department
Sandia National Laboratories
Albuquerque, New Mexico

Douglas J. Ammerman
Transportation Systems Technology Department
Sandia National Laboratories
Albuquerque, New Mexico

ABSTRACT

A series of tests investigating dynamic pulse buckling of a cylindrical shell under axial impact is compared to several 2D and 3D finite element simulations of the event. The purpose of the work is to investigate the performance of various analysis codes and element types on a problem which is applicable to radioactive material transport packages, and ultimately to develop a benchmark problem to qualify finite element analysis codes for the transport package design industry. During the pulse buckling tests, a buckle formed at each end of the cylinder, and one of the two buckles became unstable and collapsed. Numerical simulations of the test were performed using PRONTO, a Sandia developed transient dynamics analysis code, and ABAQUS/Explicit with both shell and continuum elements. The calculations are compared to the tests with respect to deformed shape and impact load history.

INTRODUCTION

Radioactive material transport packages' are required to withstand high energy impact events, which may result in large inelastic deformations, without affecting the packages ability to contain the radioactive material. The finite element method has become a well established technique for simulating these events. For U.S. radioactive material package regulators to have confidence in these analyses, it is important to have finite element based computer codes benchmarked against experiments. Hence, the Transportation Systems Technology Department at Sandia National Laboratories designed a dynamic buckling experiment for the purpose of benchmarking analysis codes against a well defined and closely monitored test which is applicable to the design and operation of radioactive material transport packages. Numerical simulations of the pulse buckling test were performed using the following analysis codes and elements to model the cylinder: PRONTO2D (Taylor and Flanagan, 1987) with axisymmetric four-node quadrilaterals; PRONTO3D (Taylor and Flanagan, 1989) with both four-node shells and eight-node hexahedrons; and ABAQUS/Explicit (HKS, 1991) with axisymmetric two-node shells and four-node quadrilaterals, and 3D four-node shells and eight-node hexahedrons. ABAQUS/Explicit is a commercial product, while the PRONTO codes were developed at Sandia National Laboratories. The inclusion of a commercial finite element code in this study was desired to demonstrate that the required tools for design based on inelastic analysis are available to any package designer. Although the geometry and load conditions of the impact event are axisymmetric, 3D calculations were performed to determine if ovaling observed in the tests was a natural buckling mode of the problem or the result of asymmetries in geometry or boundary conditions. The calculations are compared to the tests with respect to deformed shape and impact load history.

† This work was supported by the U. S. Department of Energy under Contract No. DE-AC04-94AL85000.

BENCHMARK TEST PROGRAM

Apparatus and Procedure

An illustration of the test apparatus, including component masses and dimensions, is shown in Figure 1. A series of five axial impact tests were performed on 101.6 mm-diameter, 203.2 mm-long, 304L stainless steel cylinders with a nominal 4.76 mm wall thickness. The cylinders were struck by a 271 kg mass with an impact velocity ranging from 12.9 to 13.7 m/sec. The 2200 kg support table was mounted on four hydraulic cylinders. Upper and lower platens, designed to assure a uniform impact on the flats of the cylinder, were recessed to assure alignment on center. A 0.25 in-thick felt pad was used to mitigate the acceleration spike resulting from impact so that test equipment and instrumentation would not be damaged.

DISCLAIMER

Portions of this document may be illegible in electronic image products. Images are produced from the best available original document.

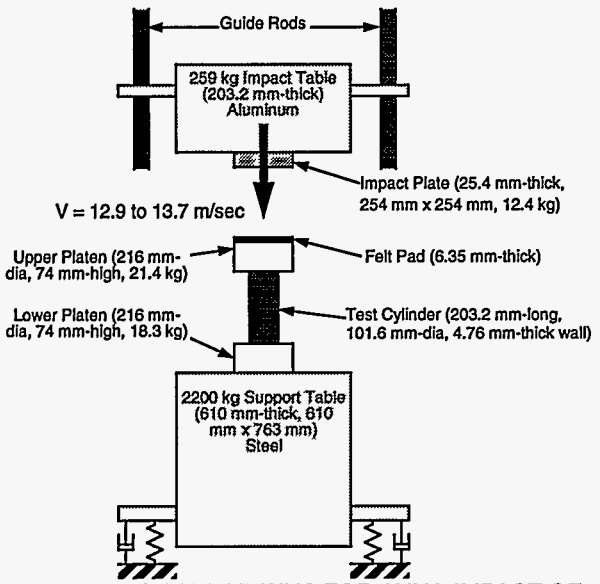

FIGURE 1. TEST APPARATUS FOR AXIAL IMPACT OF CYLINDRICAL TUBES.

Characterization of Buckling Response

Shell crushing takes place in two distinct stages, *buckling* and *collapse* (Lindberg and Florence, 1975). A buckling pattern is initiated by axial compression, taking only a few transit times of an elastic wave along the shell length to develop (approximately 0.1 ms). In the post-buckling stage, the buckles undergo large deformation collapse. This stage lasts orders of magnitude longer than the buckling stage and absorbs most of the impact energy. The principal mechanisms of energy absorption are membrane plastic flow and plastic bending. Based on an elastic stability analysis of a cylindrical shell subject to axial compression, the critical wall stress is given as:

$$\sigma_{cr} = \frac{E(h/a)}{\sqrt{3\left(1-\nu^2\right)}} \qquad (1)$$

where E is the elastic modulus, h is the wall thickness, a is the cylinder radius, ν is the Poisson's ratio. For the test cylinder geometry and material properties, this yields a critical stress of 11.4 GPa, significantly greater than the 193 MPa yield strength of 304 stainless steel. Hence, in the current problem *buckling* takes place during sustained plastic flow, a phenomena known as *plastic flow buckling* (Lindberg and Florence, 1975).

Test Results

A photograph of the four deformed test cylinders are shown in Figure 2. Examination of high speed films revealed that all of the tests exhibited the same *buckling* behavior with four nearly equally spaced buckles forming along the cylinder length (one large buckle at each end with two smaller buckles in-between). One of the end buckles became unstable and collapsed. In Tests 1, 2, and 4 the instability or *collapse* occurred at the top, while in Test 3 and the preliminary test (not shown) it occurred at the bottom. The end view shows that some of the cylinders did not buckle axisymmetrically, exhibiting a slight degree of ovaling.

TABLE 1. MATERIAL PROPERTIES FOR 304L STAINLESS STEEL

Young's Modulus (GPa)	Poisson's Ratio, ν	Yield Stress (MPa)	Hardening Constant, A (MPa)	Hardening Exponent, n
193	0.27	193	1.33	0.748

Profile measurements of the post-test cylinders are presented in Figure 3. The oval deformed shapes exhibit quarter symmetry in the circumferential direction (as seen in Figure 2). Hence, profile measurements were made at 0, 45 and 90 degrees, spanning the range of possible profiles. The zero degree profile corresponds to the circumferential position where the buckle is largest. The deformation patterns of Tests 1 and 2 are nearly axisymmetric, exhibiting small differences between the three profiles in Figure 3. However, Tests 3 and 4 pinch in one direction resulting in significant ovaling. Except for Test 3, all of the measured profiles exhibit the same four buckle profile. Test 3 yielded five buckles: one large buckle at each end and three smaller buckles in between. However, the location and relative size of the two larger buckles is in agreement with the other tests.

FINITE ELEMENT SIMULATIONS

Analysis Codes

The numerical simulations were performed with the analysis codes ABAQUS/Explicit, PRONTO2D, and PRONTO3D operating on a Cray YMP 8/864. All of the codes use an explicit time integration operator to integrate the equations of motion, and all are designed for analyzing large deformations of highly nonlinear materials subjected to high strain rates. PRONTO2D features only one element type: a four-node uniform strain quadrilateral element. PRONTO3D features two element types: an eight-node uniform strain hexahedral element and a four-node quadrilateral shell element. ABAQUS/Explicit features all three of the elements described above in addition to a two-node axisymmetric shell element which was also used in this study. The continuum elements described above use one-point integration with an hourglass control scheme to eliminate spurious deformation modes. The shell elements use numerical integration of the stress tensor through the thickness to compute the force and moment resultants. In all of the shell calculations, five integration points were specified through the thickness. The 3D shell elements use one-point integration with hourglass control to compute the stress divergence at the centroid of the element midsurface.

Constitutive Models

The 304L stainless steel test cylinder was modeled in the present calculations using a power law hardening model (Stone et al, 1990) which describes post-yield strain hardening by the following power law relationship:

$$\bar{\sigma} = \sigma_{ys} + A\bar{\varepsilon}_p^n \qquad (2)$$

where A and n are material constants, σ_{ys} is the yield stress, $\bar{\varepsilon}_p$ is the equivalent plastic strain, and $\bar{\sigma}$ is the effective stress. The material properties used for 304L stainless steel are given in Table 1 (Wellman and Salzbrenner, 1992).

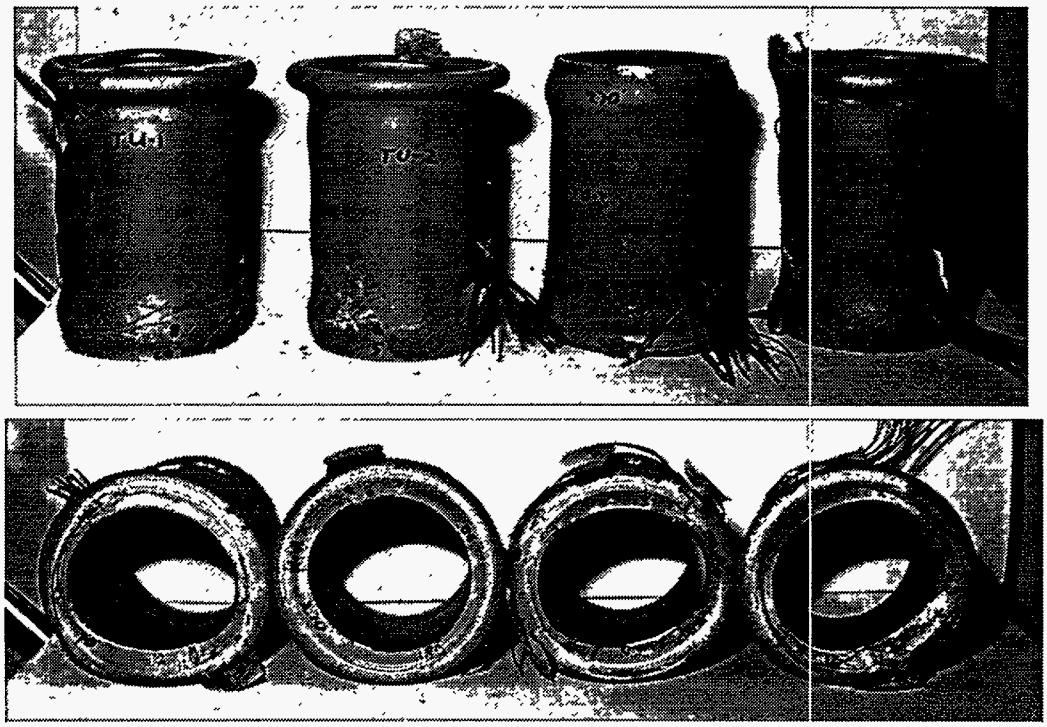

FIGURE 2. PLASTICALLY BUCKLED CYLINDERS CAUSED BY AXIAL IMPACT.

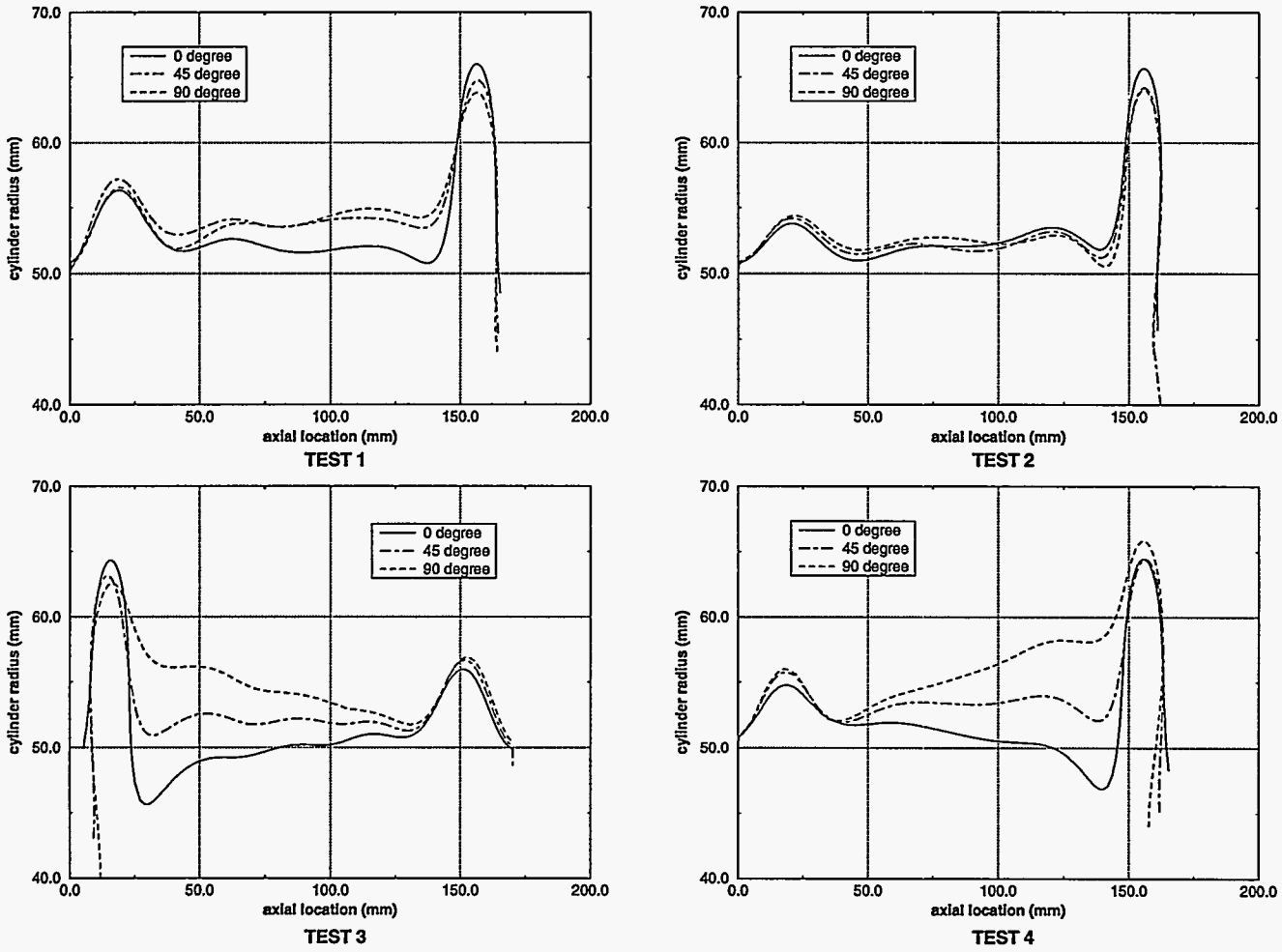

FIGURE 3. PROFILE MEASUREMENTS OF TEST CYLINDERS 1 THRU 4.

The power law hardening model is in the material library of the PRONTO codes, but not in ABAQUS/Explicit. However, in the ABAQUS/Explicit plasticity model, the stress strain relationship is defined as a piecewise linear function, allowing a close representation of Equation (2). Both models use a von Mises yield criterion with associated plastic flow and isotropic strain hardening.

To approximate the energy absorption characteristic of the felt pad, it was modeled as an elastic plastic material with properties (E = 1 GPa, hardening modulus = 138 MPa, ν = 0.0, yield strength = 0.7 MPa) such that the pad crushed to 25 percent of its original height as observed in the tests.

All other test components were modeled elastically. The impact plate, platens, and support table were fabricated from steel (E = 200 GPa, ν = 0.29) while the impact table was fabricated from aluminum (E = 68 GPa, ν = 0.33).

Geometric Models

The 2D axisymmetric finite element models used in this study are shown in Figure 4 with the cylinder modeled with (a) four-node quadrilaterals and (b) two-node shell elements. The quadrilateral model is composed of 2548 nodes and 2231 elements. The model uses five constant strain elements through the wall thickness. The use of five constant-strain elements is generally considered an acceptable compromise between accuracy and cost. The shell model is composed of 2197 nodes and 1960 elements. The nodes of the shell elements lie along the mid-wall thickness of the cylinder (r=48.42 mm). The top and bottom edges of the cylinder are 'T' shaped with two shell elements at each end for a total width of 4.76 mm, the thickness of the cylinder wall. The 'T' was necessary to enforce contact between the shells and adjacent quadrilaterals (since contact cannot be enforced along the edge of a shell element) and to correctly simulate the edge moment applied which resists the tendency for the cylinder to roll up at the edges during buckling.

The 3D models simulate the same geometry as the axisymmetric models, swept 90 degrees to produce a quarter-symmetry model. Based on preliminary calculations with a full 3D model and comparisons with the test units, quarter-symmetry was judged to

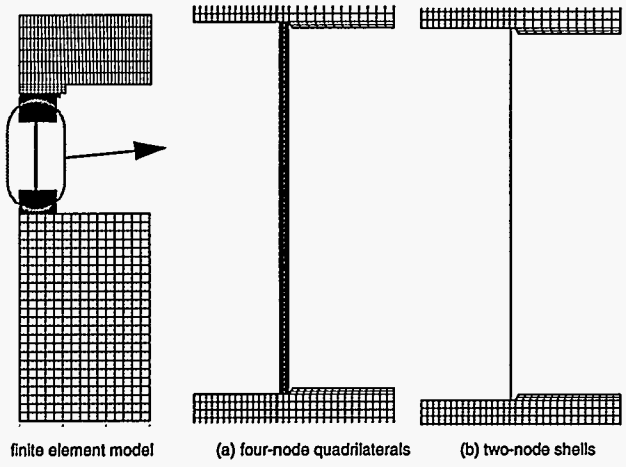

FIGURE 4. TWO DIMENSIONAL AXISYMMETRIC FINITE ELEMENT MODEL SHOWN WITH FOUR-NODE QUADRILATERAL AND TWO-NODE SHELL ELEMENTS.

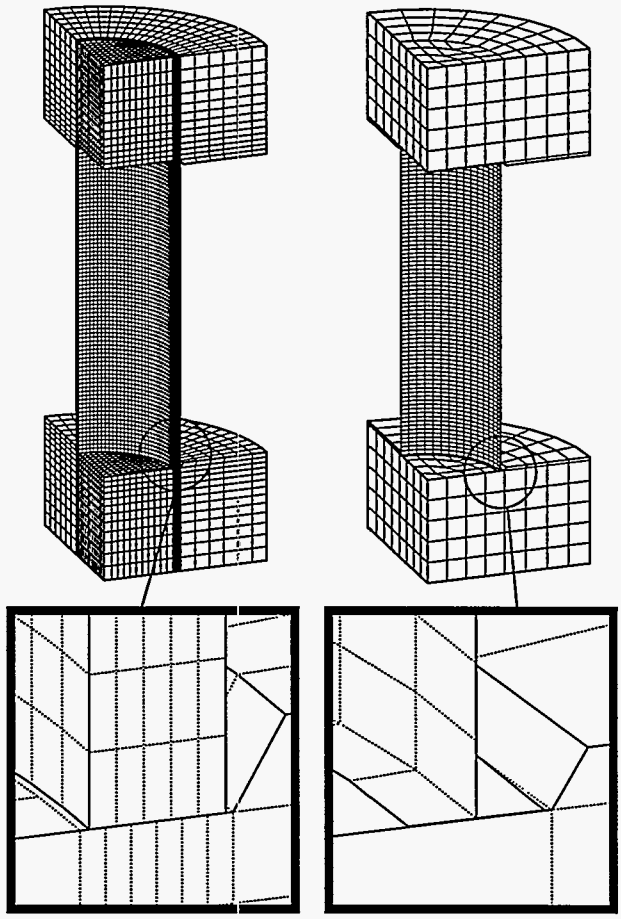

FIGURE 5. THREE-DIMENSIONAL FINITE ELEMENT MODEL SHOWN WITH CONTINUUM AND SHELL ELEMENTS.

be sufficient to capture the asymmetric buckling modes observed in the tests. The 3D finite element models of the cylinder are shown in Figure 5 with eight-node hexahedral continuum elements and four-node quadrilateral shell elements. The continuum model uses five elements through the wall thickness, 30 along the circumference, and 75 along the cylinder length. For the shell model, 15 elements were modeled along the circumference, and 75 along the cylinder length. Additional mesh refinement of the lower platen in the region of contact was required in the continuum model to quiet numerical hourglassing initiated by contact enforcement. The continuum model contains 27,591 nodes and 22,315 elements, while the shell model contains 2980 nodes and 2273 elements. The shell model also features a 'T' on the upper and lower edges.

The 2200 kg support table is supported by four hydraulic cylinders. Based on parameters of the pneumatic supports, the system was characterized to have an approximate spring constant of 193 kN/m and a 62.2 kN preload. During a test the maximum measured impact force was approximately 623 kN. At the end of the buckling event the table had only displaced 10 mm, producing 64.1 kN of spring force. Hence, for the short duration of the buckling event, the spring forces are negligible compared to the inertial forces and are therefore neglected in the simulations.

Simulation of the Buckling Event

The buckling event is shown in Figure 6 for the PRONTO3D shell calculation. At 1.3 ms into the simulation, two buckles of nearly equal size develop at the upper and lower ends of the cylinder at approximately the same distance from each end. By 2.5 ms, both buckles have grown, with the upper buckle becoming slightly larger. By 4.0 ms the upper buckle has become unstable and by 7.0 ms has collapsed.

The inability to reproduce identical post-buckling results in all of the tests raised concerns with respect to the multiplicity of solutions and how that might affect a numerical benchmarking exercise. There are two distinct post-buckling results observed in the tests: one in which the instability occurs on top and the other in which the instability occurs on the bottom. However, a closer investigation of the computed post-buckling behavior reveals that the two results are mechanistically similar. Hence, the two post-buckled shapes represent only one test result.

The radial displacements of nodes on the apex of each of the larger buckles and on the cylinder mid-length are plotted as a function of time in Figure 7 for the PRONTO3D shell calculation. Early in the event (less than 1.5 ms), the location of the largest radial displacement alternates from top to bottom. The velocity of the upper platen is also shown in Figure 7. The cyclic velocity history indicates that the impact table bounces on the upper platen. Each impact causes the upper buckle to become the largest. During rebound of the impact table, the lower buckle overtakes the upper. Because of mid-length expansion of the shell, the applied load becomes eccentric relative to the shell wall, resulting in a bending moment being applied to the shell wall. As the buckles form, a hardening moment develops (due to differential stress states through the wall thickness) which resists further curvature increases. Instability occurs when the applied bending moment is greater than the hardening moment, causing the largest of the two buckles to become unstable and collapse. In performing the calculations, it was observed that if the instability occurs during impact, the upper buckle becomes unstable; whereas if the instability occurs during rebound, the lower buckle becomes unstable. The rebound characteristics of the impact table, and

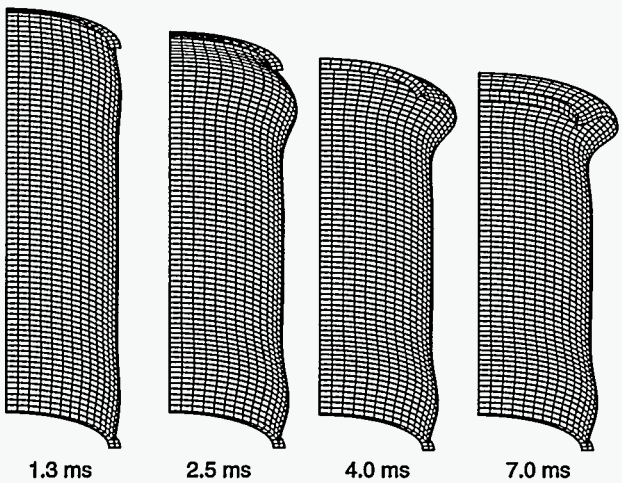

FIGURE 6. DEFORMED SHAPES OF CIRCULAR TUBE DUE TO AXIAL IMPACT.

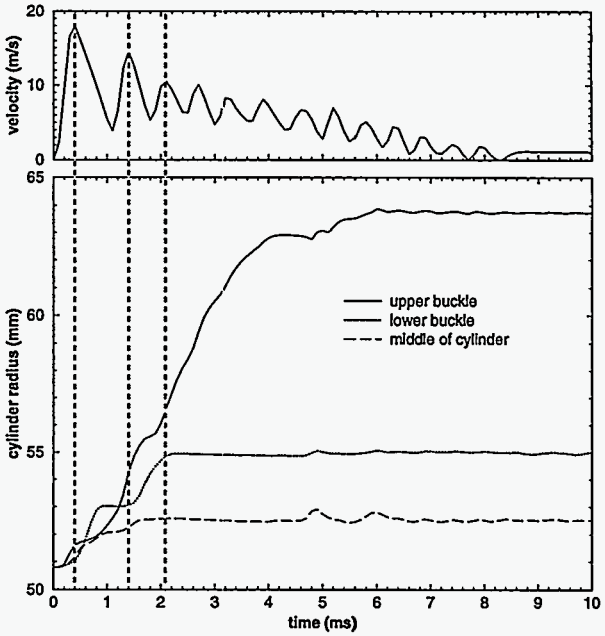

FIGURE 7. (A) VELOCITY OF UPPER PLATEN, AND (B) RADIAL GROWTH OF THE END-BUCKLES AND THE CYLINDER MID-LENGTH AS A FUNCTION OF TIME.

hence the location of the buckling instability, were found to be sensitive to the felt pad properties. However, the two post-buckled shapes were identical, only inverted top-to-bottom. Hence, based on numerical investigation, it is proposed that the two post-buckled shapes observed in the tests represent mechanistically similar if not identical solutions.

COMPARISON OF ANALYSIS RESULTS WITH DATA

Final Deformed Shape

All four of the 3D calculations yielded an axisymmetric buckling pattern. Hence, the seven computed profiles are compared to the profile of Test 2 which buckled nearly axisymmetrically. The final deformed profiles of the shell element calculations are compared in Figure 8 to the test unit. The shell models show reasonably good agreement with the test. The calculations predict the development of two dominant buckles at the top and bottom of the cylinder. All of the shell models predicted that the buckling instability would occur at the top of the cylinder except for the axisymmetric model which predicted the instability would occur at the bottom. The calculations show good agreement with the test with respect to the size and location of the upper and lower buckles. However, the ABAQUS 3D shell calculation did not completely collapse in contrast to the other two shell calculations. All three of the shell calculations were determined to be convergent solutions based on mesh refinement studies. The two smaller buckles in-between the larger buckles are not as evident in the simulations as in the test unit. The PRONTO3D shell element calculation shows the two smaller buckles most clearly. However, the smaller buckles are present in all of the shell element calculations as is evident by the correct spacing of the larger buckles. Three buckles would result in the

larger buckles being positioned farther from the ends. The smaller buckles are more visible at earlier times in the simulations. As the simulations progress the cylinder bulges at the middle, making the two smaller buckles appear more like one.

The final deformed profiles of the continuum element calculations are compared in Figure 9 to the profile of the test unit. Both of the 3D hex calculations and the ABAQUS axisymmetric quad calculation do not agree very well with the test unit. The bending response of the shell walls in these calculations was too stiff, resulting in only three equally spaced buckles. The stiffness in these models inhibited the development of the buckling instability. These calculations also show greater radial expansion at mid-length. Conversely, the PRONTO2D axisymmetric calculation (with the same mesh refinement as the ABAQUS axisymmetric model) showed reasonably good agreement with the test. Also shown in the plot are the results of the ABAQUS axisymmetric quad calculation run with a finer mesh using 11 elements through the thickness and 200 along the length (vs. 5 by 75). The results of this calculation compare much more favorably with the test. This raises concerns as to why different mesh

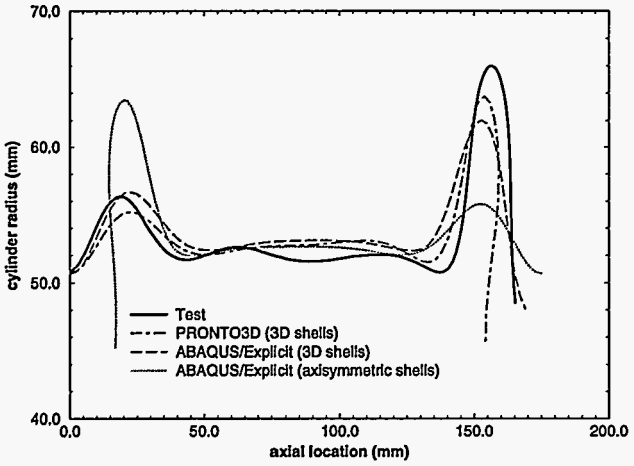

FIGURE 8. PROFILES OF SHELL ELEMENT CALCULATIONS COMPARED TO TEST.

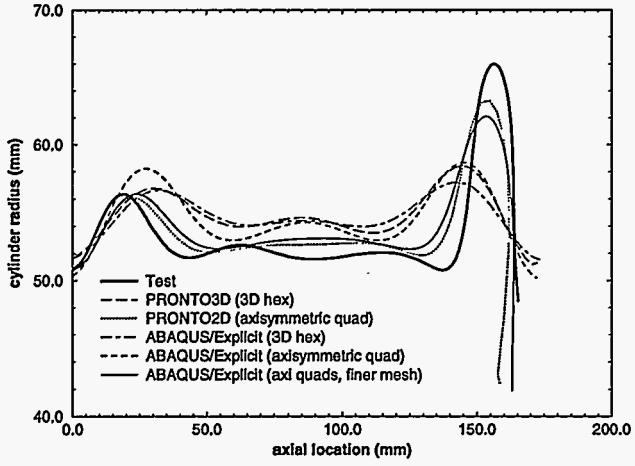

FIGURE 9. PROFILES OF CONTINUUM ELEMENT CALCULATIONS COMPARED TO TEST.

refinement is required for analysis codes using similar element technology. This may be due to differences in the hourglass control formulations of the two codes. Bending deformations, such as those predicted at the collapse region, activate the hourglass deformation mode of an element (Flanagan and Belytschko, 1981). If the artificial hourglass stiffness is too high, then bending would be inhibited. Unfortunately, there is no user control of hourglass stiffness in ABAQUS. The only way to decrease the effect of the artificial hourglass stiffness is to increase mesh refinement. Hence, five elements through the tube wall thickness is not necessarily adequate for all codes and element types.

Neither of the 3D continuum models were run with finer meshes due to computational expense. However, it is reasonable to expect a similar improvement in performance with further mesh refinement.

Dynamic Load Comparison

The predicted load histories of the various finite element simulations are compared in Figure 10 to the measured load history. The results are presented in three plots for clarity. The measured impact load history is representative of all of the tests as the measurements were very consistent from test-to-test (no variations were detected due to location of the buckling instability). The maximum measured load was approximately 600 kN. The load decreases, as the larger buckle becomes unstable, to 300 kN and then increases again to a second peak of 400 kN as the buckle collapses (the outer wall contacts the platen). The first plot shows the load history of the continuum element models which are too stiff. In all of these calculations, the predicted maximum load is greater than the measured load. Because these models are too stiff to collapse, they do not predict a second load increase. The ABAQUS 3D shells model accurately predicts the maximum load (as one of the buckles becomes unstable) but does not predict a second increase since the buckle did not fully collapse. Both the ABAQUS axisymmetric shells and axisymmetric quads (finer mesh) yielded similar results. They accurately predict the maximum load, the load decrease due to collapse, and the second load increase. However, the second increase comes much later than the test data, indicating a slightly stiff response which does not allow the buckle to collapse as quickly. The best agreement with the test data was obtained with the PRONTO2D axisymmetric continuum and PRONTO3D shells models. Both of these models accurately predicted the maximum load, the decrease due to instability, as well as the timing of the second increase.

Asymmetric Buckling

The original goal was to develop an axisymmetric benchmark problem. It was not certain whether the oval buckling observed in some of the tests was an asymmetric buckling mode, or the result of asymmetries in the test. To determine the effect of asymmetric boundary conditions on buckling performance, a 3D shell calculation was run using PRONTO3D with asymmetric friction along the tube/platten interfaces. The quarter symmetry model shown in Figure 5 was used with a cofficient of friction of 0.1 over 45 degrees of the contact surface and 0.2 over the remaining 45

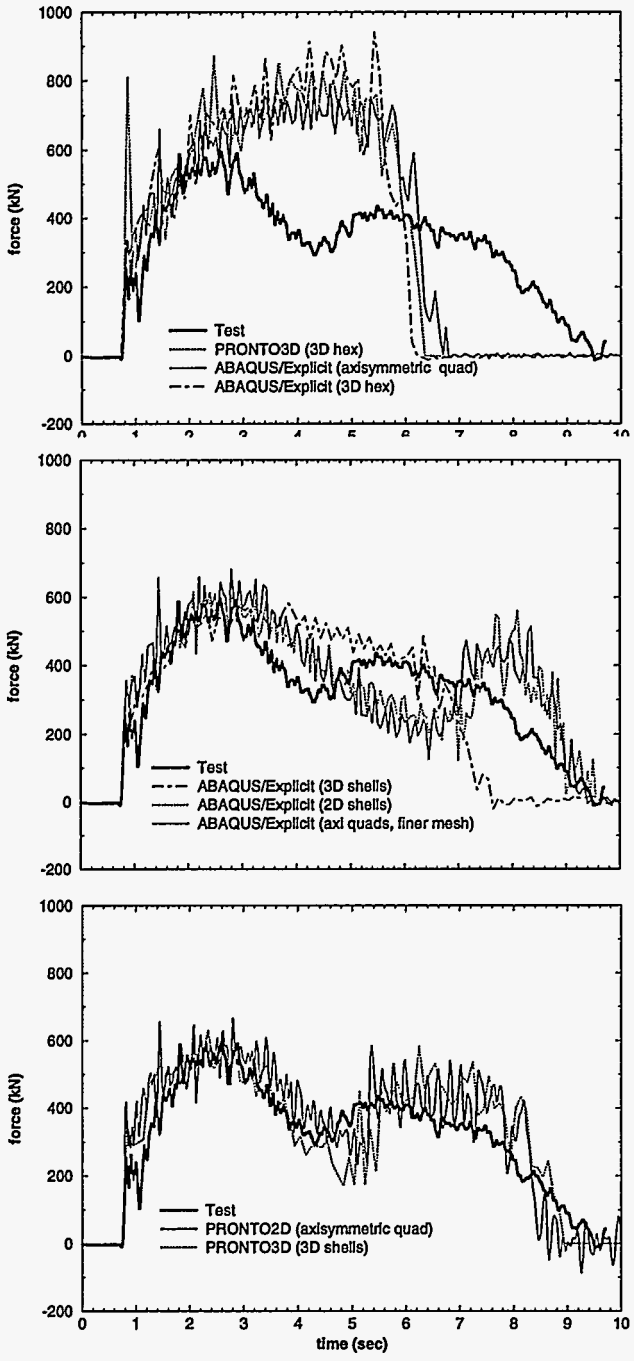

FIGURE 10. CALCULATED LOAD HISTORIES COMPARED TO TEST DATA.

degrees. The computed profile is plotted in Figure 11. The profiles are consistent with the deformed shapes of Tests 1, 3, and 4 (Figure 3). Hence, the ovaling observed in some of the tests appears to be due to asymmetries of this kind.

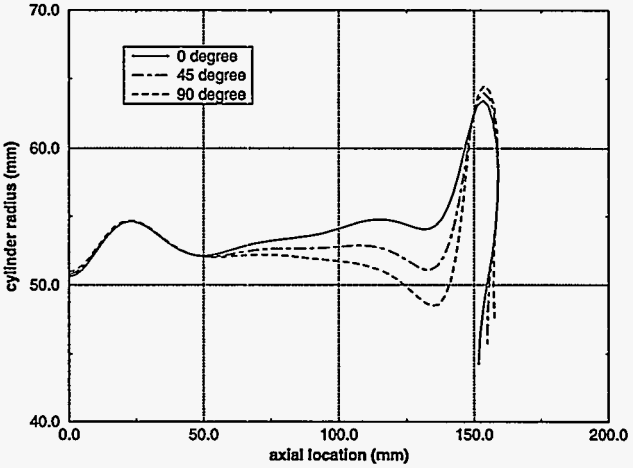

FIGURE 11. PROFILES OF 3D SHELL CALCULATION WITH ASYMMETRIC BOUNDARY CONDITIONS.

Computing Cost Comparison

The computing costs are presented in Table 2. The following observations are presented:

(1) The ABAQUS/Explicit calculations were consistently more expensive than the corresponding PRONTO calculations. This was expected since ABAQUS is a general purpose finite element code which carries additional overhead for its abundant features and element types.

(2) The shell element calculations were less expensive than the continuum element models because they required fewer elements and the critical time step for these models is twice that of the continuum models. The critical time step for an explicit time integration scheme is proportional to the smallest element dimension. In the continuum models, the smallest element dimension is through the wall thickness, which is not discretized in the shell models.

(3) The ABAQUS axisymmetric quadrilateral model with the finer mesh required four times the CPU time of the coarse mesh. A comparable increase in computing expense for the 3D continuum models would be prohibitively expensive.

TABLE 2. SUMMARY OF CALCULATIONS AND CPU RUN TIME (RUN ON CRAY YMP 8/864)

Analysis Code	Element Type	CPU time (hr)
PRONTO2D	axisymmetric quad	.34
PRONTO3D	3D hex	11.2
	3D shell	1.37
ABAQUS/Explicit	axisymmetric shell	.33
	axisymmetric quad	1.37
	axisymmetric quad (finer mesh)	3.0
	3D hex	38
	3D shell	1.7

DISCUSSION AND CONCLUSIONS

This study demonstrates that experiments, typically accepted as the correct answer, can have multiple results due to sensitivities inherent in the test design. Often times benchmark problems are based on a single test. Calculations which produce different results from the test are quickly dismissed as being incorrect. By performing multiple tests, the unstable nature of the problem was experimentally confirmed.

A good benchmark problem should have a single, repeatable solution. The variability in the experimental results of this study suggests the problem has multiple solutions. Complexities in the test design, such as the felt pad, proved difficult to model yet had a significant effect on the experimental results. Although the original intent was to provide an axisymmetric benchmark, asymmetries in the boundary conditions produced asymmetric results. Such complexities obscure the basic mechanics of the problem which are of greatest interest. However, it was determined that all of the tests are mechanistically similar if not identical. Hence, the tests provide a good benchmark of the dynamic buckling problem. It can be argued that it is not necessary to include all of the complexities of the experimental problem (felt pad, geometric asymmetries, etc.) in the benchmark. Once it has been demonstrated that one code can accurately capture the mechanics of the experiment, future benchmarking can be performed using the exact geometry and boundary conditions of that numerical model rather than the uncertain experimental results.

All of the evaluated codes predicted dynamic buckling without the inclusion of material or geometric imperfections. This indicates that finite element analysis is a good tool for inelastic design of transportation packages subject to dynamic buckling conditions, one of the most difficult conditions to analyze. In addition, valuable insight was provided into solving dynamic pulse buckling problems. For example, it is not necessarily true that five constant-strain elements through the shell thickness represents an acceptable compromise between accuracy and cost. This is a generally accepted guideline based on the fact that four to five constant-strain elements are sufficient to capture a bending stress distribution. The computational results presented here demonstrate that, although two analysis codes use similar element types, each may require different mesh refinement to produce a convergent solution. The use of PRONTO2D with axisymmetric quadrilaterals required five elements through the shell thickness, while the use of similar axisymmetric quadrilateral elements with ABAQUS/Explicit required eleven. Similarly, the 3D continuum calculations were not convergent with five elements through the thickness. Further refinement of the mesh would probably improve the results, but would be prohibitively expensive. Furthermore, the discrepancies may be characteristic of the analysis code or element type, such as the ABAQUS 3D shell elements which were stiffer than PRONTO3D shell elements. These results should provide insight and guidance for the structural analysis of transportation casks.

REFERENCES

Taylor, L. M., and Flanagan, D. P., 1987, "PRONTO2D: A Two-dimensional Transient Solid Dynamics Program," Technical Report SAND86-0594, Sandia National Labs, Albuquerque, NM.

Taylor, L. M., and Flanagan, D. P., 1989, "PRONTO3D: A Three-dimensional Transient Solid Dynamics Program," Technical Report SAND87-1912, Sandia National Labs, Albuquerque, NM.

ABAQUS/Explicit Users' Manual, 1991, Hibbitt, Karlson, and Sorensen, Inc.

Stone, C. M., Wellman, G. W., and Krieg, R. D., 1990, "A Vectorized Elastic-Plastic Power Law Hardening Material Model Including Lüders Strain," Technical Report SAND90-0153, Sandia National Laboratories, Albuquerque, NM.

Wellman, G. W., and Salzbrenner, R., 1992, "Quasistatic Modeling and Testing of Exclusion Region Barrier Mock-Ups," Technical Report SAND92-0024, Sandia National Labs, Albuquerque, NM.

Lindberg, H. E., and Florence, A. L., 1987, "Dynamic Pulse Buckling," Martinus Nijhoff Pubs., Dordrecht, The Netherlands.

Brush, D. O., and Almroth, B. O., 1975, "Buckling of Bars, Plates, and Shells," McGraw Hill, New York.

Flanagan, D. P., and Belytschko, T., 1981, "A Uniform Strain Hexahedron and Quadrilateral with Orthogonal Hourglass Control," *Intern. Jour. for Num. Methods in Eng.*, Vol. 17.